IJEM INTERNATIONAL JOURNAL OF Electroactive Materials

Int. J. Electroactive Mater. 4 (2016) 33 – 38
www.electroactmater.com

Characterization and Performance of Porous Chitosan Membrane for Proton Batteries

Siti Salwa Alias*, Zulkifli Mohamad Ariff, Ahmad Azmin Mohamad

School of Materials and Mineral Resources Engineering, Universiti Sains Malaysia, 14300 Nibong Tebal, Pulau Pinang, Malaysia
*E-mail Address: ssalias86@gmail.com

Received: 6 December 2016 / Accepted: 30 December 2016 / Published: 31 December 2016

ABSTRACT: A porous chitosan membrane was prepared by using an ultrasonic mixed phase inversion and solution-cast method using silica as the porogent agent and sodium hydroxide solution as the porogent remover. The porous chitosan membrane was soaked in 5.0-M ammonium acetate electrolyte for 48 hours. Several functional groups shifted, and the existence of an NH_3^+ deformation peak (1540 cm^{-1}) proved that interaction had taken place between the chitosan and ammonium acetate. A thermal analysis revealed that the porous chitosan membrane was suitable for use at room temperature and up to 60 °C. The tensile strength (1.2 MPa), modulus of elasticity (5.7 MPa) and elongation at break (14.5 %) met the minimum requirements for the use of membranes in batteries. The fabrication and comparison of the performance of two coin cell proton batteries combined in a series and connected to a green light emitting diode showed a correlation between the actual output voltage (2.6 V) and the simulation voltage (2.1 V). These results confirmed that the porous chitosan membrane had good properties and was suitable for use as a polymer electrolyte for proton batteries.
Keywords: Porous chitosan membrane; Functional group; Thermal; Tensile; Proton batteries; Simulation

1. Introduction

Chitosan has been used as a proton-conducting polymer electrolyte for the past decade [1-3]. Numerous modifications have been done to improve the properties of the chitosan proton-conducting polymer electrolyte, i.e. the addition of various types of salts [1, 4], plasticizers [2, 5], fillers [6, 7], cross-linkers [8, 9], and the blending of chitosan with other polymers [10, 11]. However, previous studies focused on improving the ionic conductivity values, and were lacking in several characterizations, such as chemical interactions, thermal stability and tensile strength, in a single comprehensive report.

Besides that, most of the previous studies used the chitosan proton-conducting polymer electrolyte in solid form. The drawback of a solid chitosan electrolyte is its poorer ability to absorb water (~ 95 %) compared with porous chitosan (~173 %) [12]. The existence of pores inside the chitosan membrane improves the electrolyte uptake (308.6 %) [13], ionic conductivity (3.6×10^{-3} S cm^{-1}), and electrochemical potential stability window (3.8 V) [14]. However, the majority of the studies on porous chitosan membranes focused mainly on fuel cell applications and performance [9, 15, 16].

In fact, previous studies on the chitosan proton-conducting polymer electrolyte were limited with regard to mixing with other materials or various types of characterizations without specific applications [17-20]. Since 2005, only eight proton batteries based on chitosan proton-conducting polymer electrolytes have been fabricated over eleven years of research [2, 4, 10, 13, 21-24]. The comparison between the simulation and the actual performance is also important, particularly after being connected to a load. However, no studies have been carried out to compare the actual and the simulation performance of proton batteries.

Therefore, the first goal of this study was to produce a porous chitosan membrane via an ultrasonic mixed phase inversion and solution-cast method, and to characterize the functional groups, and the thermal and tensile properties. The second goal was to fabricate a porous chitosan membrane as an electrolyte for proton batteries and to compare the actual and simulation performance of coin cell proton batteries connected to a light-emitting diode (LED).

2. Experimental

2.1 Porous Chitosan-NH_4CH_3COO: Preparation and characterization

A porous chitosan membrane (PCA) was prepared by an ultrasonic mixed phase inversion and solution-cast method [13, 14], and was used as the control sample. The PCA was soaked in a 5.0-M ammonium acetate (NH_4CH_3COO) electrolyte for 48 hours (PCA-5A), as explained in detail earlier [14]. The functional groups of the NH_4CH_3COO electrolyte, PCA and PCA-5A membranes were analysed using Fourier transform infrared spectroscopy (FTIR, Perkin-Elmer®) with a wave number of between 4000 and 550 cm^{-1} and a resolution of 4 cm^{-1}. The chemical interaction was sketched using ChemDraw Ultra 8.0.

The thermal stability of the PCA and PCA-5A membranes were determined based on their weight loss at a certain temperature by using thermogravimetric-derivative thermogravimetric analysis (TGA-DTG, Perkin Elmer®). The PCA and PCA-5A membranes (10.0 mg) were placed in alumina crucibles, and were subjected concurrently to a temperature range of between 35 to 800 °C. All the measurements were conducted under an inert nitrogen atmosphere at a heating rate of 10 °C min^{-1} to avoid oxidation of the samples. From the TGA curves, the

characteristic temperatures of the initial and maximum decompositions were determined.

The tensile properties of the PCA and PCA-5A membranes were determined by using a tensile test (Testometer M 500). The tensile test was conducted based on ISO 527-3 at a testing speed of 50.0 mm/min using dumbbell specimens with a width of 5.0 mm cut from a moulded sheet. Five membranes were used for each test and the average value was taken with regard to the tensile properties.

2.2 Proton Batteries: Fabrication and simulation

The proton batteries were fabricated as Zn + $ZnSO_47H_2O$ + Super P + PTFE || PCA-5A membrane || MnO_2 + Super P + PTFE coin cell [13]. Two coin cells were combined and connected in series to turn on the green LED for the actual proton batteries. A virtual electronic simulation using MULTISIM was also employed to compare the simulation performance with that of the actual proton batteries. All the components and circuits were designed to be similar to the actual ones. The input value of each virtual coin cell was set at 1.5 V, 0.03 Ω, and 11.7 mA h based on the prior open circuit voltage (OCV), current-voltage (*I-V*) and discharge profile data, respectively [13].

3. Results and discussions

3.1 Functional groups and chemical interaction

The existence and shifting of the functional groups in the PCA and PCA-5A membranes were important to prove that protonation occurred due to the shifting of $–NH_2$ to $–NH_3^+$ after having been soaked in the 5.0-M NH_4CH_3COO electrolyte (**Figure 1a-d**). In the region of 3800-2200 cm^{-1}, the broad peaks (3600-3050 cm^{-1}) of the PCA membrane referred to the N–H and O–H bands [25-27]. The two peaks that were present in the region of 1800-1200 cm^{-1} were the C–O–NHR band and the NH_2 deformation of amine. In the region of 1200-900 cm^{-1}, the peaks were assigned to the C–O stretch, C–O–C bending vibration of the glucose rings and the glycosidic linkages. Another two peaks (990 and 928 cm^{-1}) were assigned to the C–O–H deformation of the O–H bending. All the FTIR peaks of the PCA membrane were similar to those in a previous study on chitosan membranes [21, 27-29].

Meanwhile, for the NH_4CH_3COO electrolyte, only one peak (C–H stretch) was revealed in this region (3800-2200 cm^{-1}). Four peaks were present in the region of 1800-1200 cm^{-1}, namely the N–H bend, CH_3 deformation, C=O symmetrical stretching and C-H deformation bend. The three peaks revealed in the region of 1200-900 cm^{-1} were

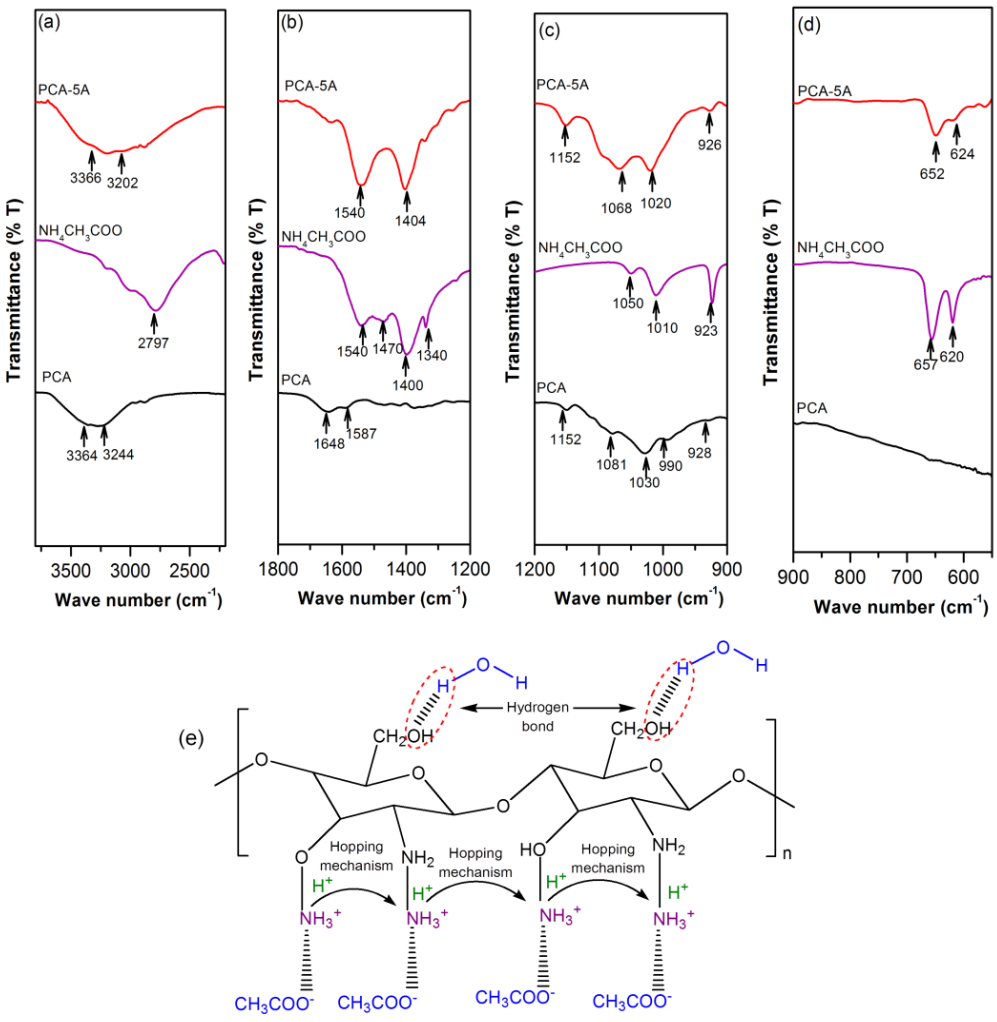

Figure 1: (a) FTIR spectra of PCA membrane, ammonium acetate, PCA-5A membrane in different regions of 3800-2200 cm^{-1}, (b) 1800-1200 cm^{-1}, (c) 1200-900 cm^{-1}, (d) 900-550 cm^{-1}, and (e) interaction between PCA-5A membrane and ammonium acetate electrolyte

assigned to the C–O stretch. In the region of 900-550 cm^{-1}, the peaks referred to the O–C–O bend of the COOR. The FTIR data of the NH_4CH_3COO were supported by the literature [30].

After being soaked in the 5.0-M NH_4CH_3COO electrolyte, both the PCA-5A membrane peaks (3364 and 3244 cm^{-1}) shifted (3366 and 3202 cm^{-1}) due to the symmetric and asymmetric N–H bands and the stretching vibration from the intra and inter-molecular hydrogen bonds of O–H [25-27]. The disappearance of the NH_4CH_3COO peak (2797 cm^{-1}) indicated that interaction had occurred between the PCA-5A membrane and the NH_4CH_3COO. Two peaks were exhibited in the region of 1800-1200 cm^{-1}. The peak at 1540 cm^{-1} was assigned to the deformation of NH_3^+.

The shifting of the NH_4CH_3COO peak at 1400 cm^{-1} to 1404 cm^{-1} (symmetrical stretching of C=O) indicated the absorption of NH_4CH_3COO into the PCA-5A membrane. The shift of the C=O bond to a higher wave number was due to the increase in the force constant of the C=O bond [30]. Few peaks were depicted in the region of 1200-900 cm^{-1} for the PCA-5A membrane. The C–O stretched peak of the chitosan remained unchanged. The peaks at 1081 and 1030 cm^{-1} (C–O–C bending vibration) shifted (1068 and 1020 cm^{-1}), while the peak at 928 cm^{-1} (C–O–H deformation) also shifted (926 cm^{-1}). In the region of 900-550 cm^{-1}, two peaks of NH_4CH_3COO at 657 and 620 cm^{-1} (O–C–O bend) shifted (652 and 624 cm^{-1}). The shifting of these peaks confirmed the interaction between the PCA-5A membrane and NH_4CH_3COO.

The conducting species in this work were the H^+ ions, similar with the previous study by Hashmi et al. [31]. This indicated that the H^+ ions that originated from the NH_4CH_3COO had been absorbed by the PCA-5A membrane, and that the conduction had occurred via the Grotthuss mechanism [28]. One of the four hydrogen atoms with the weakest bond in the NH_4^+ ion was able to dissociate easily under the influence of an electric field. This H^+ ion could hop from one site to another, leaving a vacancy which was filled by another H^+ ion from a neighbouring site (**Figure 1e**).

The three polar functional groups, namely the –OH, $–NH_2$ and C–O–C groups, along the backbone demonstrate that chitosan has high water-attracting capacity to form hydrogen bonds ($CH_2OH–OH_2$, $OH–OH_2$ and $NH_2–H_2O$) [32-34]. Meanwhile, a specific platform for side group attachments under mild reaction conditions is provided by the active primary amine ($–NH_2$). Since $–NH_2$ is positively charged, hence it will be attracted to the anionic ions ($COOH^-$) and will bind and bridge with them [35]. This is similar to previous FTIR results for chitosan-NH_4NO_3 and chitosan-NH_4I [5, 28].

However, this study focused on the ability of the NH_4CH_3COO electrolyte solution to be absorbed by the PCA-5A membrane rather than the production of polymer-salt complexation. The absorption of NH_4CH_3COO into the pores of the membrane occurred externally during the soaking process. In addition, the FTIR results were also correlated with the conductivity results. There was also not much change in the conductivity values (in range of 10^{-3}-10^{-4} S cm^{-1}) [13, 14]. Details on the shifting of the PCA and PCA-5A membrane functional groups are summarized in **Table 1**.

Table 1: Functional groups of PCA membrane, ammonium acetate and PCA-5A membrane

Sample	Wave number (cm^{-1})	Functional group
PCA	3364	N–H stretch
	3244	O–H stretch
	1648	C–O–NHR band
	1587	NH_2 deformation
	1152	C–O stretch
	1081	C–O–C bending vibration
	1030	C–O–C bending vibration
	990	C–O–H deformation
	928	C–O–H deformation
NH_4CH_3COO	2797	N–H stretch
	1540	N–H bend
	1470	CH_3 deformation
	1400	C=O stretch
	1340	CH_3 deformation
	1050	C–O stretch
	1010	C–O stretch
	923	C–O stretch
	657	O–C–O bend
	620	O–C–O bend
PCA-5A	3366	N–H stretch
	3202	O–H stretch
	1540	NH_3^+ deformation
	1404	C=O stretch
	1152	C–O stretch
	1068	C–O–C stretch
	1020	C–O–C bending vibration
	926	C–O–H deformation
	652	O–C–O bend
	624	O–C–O bend

3.2 Thermal stability

The TGA-DTG analysis was important for determining the thermal stability and the degradation of the PCA and PCA-5A membranes. The weight loss of the PCA membrane was divided into three stages (**Figure 2a**). Stage I, within the range of between 30 and 100 °C (decomposition temperature of 70 °C), referred to the evaporation of water from the membrane. The range for stage II was divided into two parts, including 101-230 °C (decomposition temperature of 210 °C) and 221-320 °C (decomposition temperature of 280 °C). This referred to the degradation of the side-chains and backbone of the chitosan. Stage III (321-700 °C) indicated the continued degradation of the chitosan backbone and all the components.

Meanwhile, for the PCA-5A membrane, a large TGA curve and decomposition temperature peaks (80 °C) could be seen at Stage I (30-210 °C), indicating a higher weight loss compared to the PCA membrane (**Figure 2b**). The rapid weight loss and the decomposition temperature in Stage I were attributed to the increasing amount of NH_4CH_3COO electrolyte that was being absorbed into the membrane. The interconnected pores may have been the reason for the continuous loss in weight of the membrane [36]. Although a large amount of electrolyte was absorbed

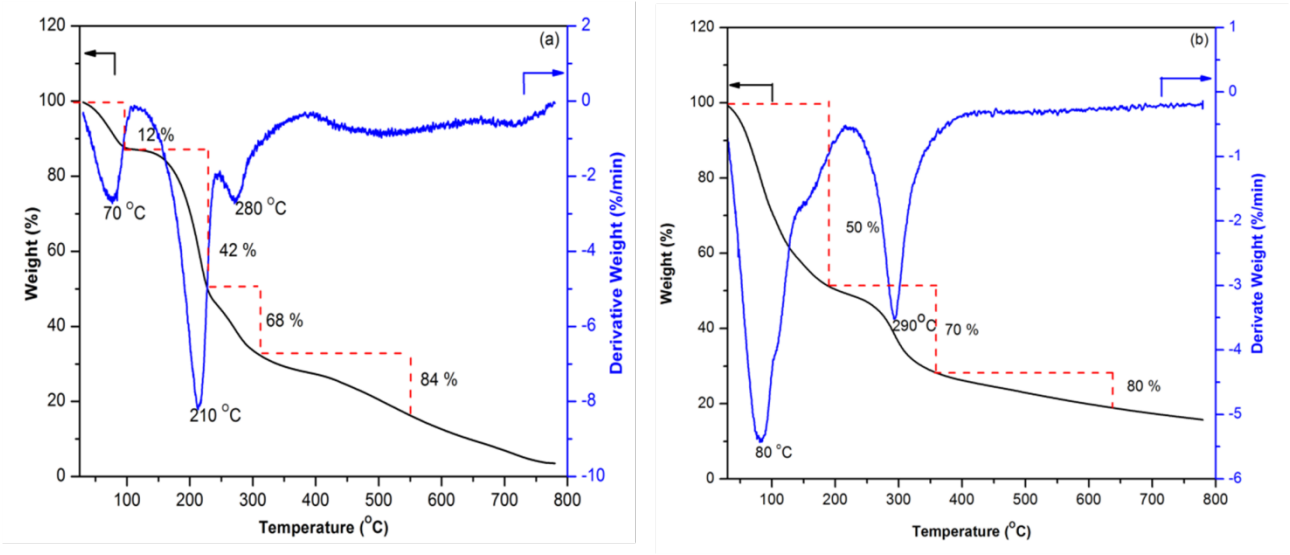

Figure 2: TGA-DTG curves for (a) PCA, and (b) PCA-5A membranes

into the PCA-5A membrane, the large, open pore layer was not suitable for the retention of the electrolyte at elevated temperatures. Hence, the NH_4CH_3COO electrolyte inside these pores was able to evaporate naturally with a slight increase in temperature, similar to a prior study on porous PVDF-HFP membranes for lithium battery applications [36].

The weight loss in the PCA-5A membrane at Stage II (211-340 °C) with a decomposition temperature peak at 290 °C was also higher compared to that of the PCA membrane. After being soaked in the NH_4CH_3COO electrolyte, the moisture content of the PCA-5A membrane increased, promoting higher dehydration of the saccharide rings, depolymerisation and decomposition of the chitosan backbone, including the acetylated and deacetylated units in Stage II. The weight loss of the remaining components and the degradation of the chitosan backbone continued to increase in Stage III (341-700 °C).

The PCA-5A membrane also had a higher residual weight compared to the PCA membrane. This was due to the trapped solvent within the polymer structure, as this is not characteristic of the polymer phase [37]. Generally, the porous polymer membrane with smaller-sized pores has much more compacted pore layers. This structure can efficiently suppress the evaporation of the liquid electrolyte when the temperature increases slightly. Most of the liquid electrolyte is stored inside [36]. However, at room temperature and up to 60 °C, the PCA-5A membrane still exhibited a good retention of the NH_4CH_3COO electrolyte, and therefore, is suitable for use as an electrolyte for proton batteries.

3.3 Tensile properties

The tensile properties, including tensile strength, modulus of elasticity and elongation at break, are important characterizations for determining the flexibility of the PCA and PCA-5A membranes based on the stress-strain curves. The small plastic region of the PCA membrane in the stress-strain curve denoted that this membrane is brittle, based on the tensile strength value of 2.0 MPa, and the modulus of elasticity of 6.0 MPa, but has sufficient flexibility of 9.2 % (**Figure 3**).

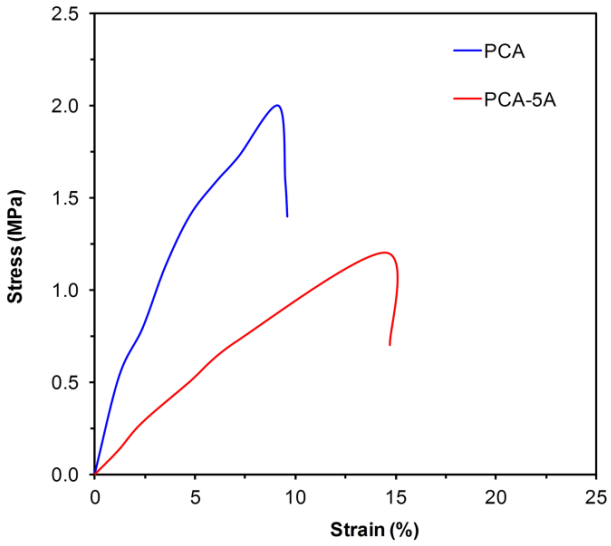

Figure 3: Stress-strain relation of PCA and PCA-5A membranes

After being soaked in the NH_4CH_3COO electrolyte, the stress-strain curve of the PCA-5A membrane showed a large plastic region. The tensile strength (1.2 MPa) and modulus of elasticity (5.7 MPa) decreased, but the elongation at break (14.5 %) increased. This indicated that the greater amount of NH_4CH_3COO electrolyte that had been absorbed into the PCA-5A membrane enabled the H^+ ions to move freely inside the membrane. The chitosan chains were less intact, and the friction between the chains was reduced. Hence, the PCA-5A membrane became more flexible, the tensile strength and modulus of elasticity were reduced, and the elongation at break increased.

According to Zhang et al. [38], the tensile strength value need not necessarily be lower than 1.1 MPa for battery applications. Although the tensile strength for the PCA-5A membrane was lower, it still met the minimum requirement of tensile strength for batteries. The value of the tensile strength was comparable with the value of the tensile strength of the chitosan membrane for electrochemical devices (1.2-4.1 MPa) [39]. In fact, the

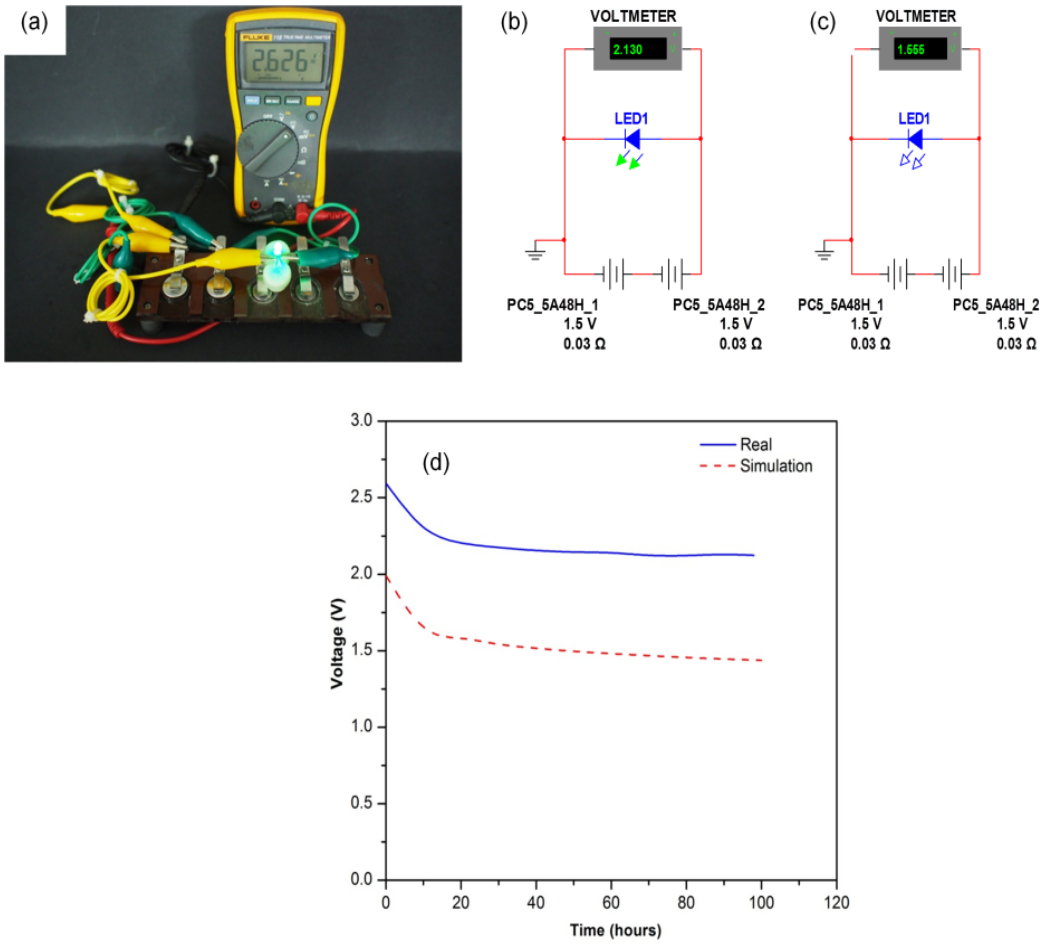

Figure 4: (a) Actual functioning of coin cell proton batteries connected in series with green LED, (b) simulation of coin cell proton batteries using MULTISIM during testing, (c) after completion of the testing, and (d) output voltage of actual and simulation coin cell proton batteries connected in series with green LED

main issue here was to obtain the tensile properties in terms of specific values to withstand the tension of the winding membrane during the fabrication of proton batteries. Based on all the characterizations that have been discussed, the PCA-5A membrane is suitable for fabrication as an electrolyte for coin cell proton batteries.

3.4 Performance of proton batteries: Actual and simulation

It is important to determine the output voltage of coin cell proton batteries as the lifespan and the performance of the batteries are sensitive to the discharging parameters [40]. The output voltage for a green LED (2.6 V) connected to two coin cell proton batteries in series confirmed that the proposed circuit was valid since a minimum voltage of 1.9 V was needed to turn on the green LED in series (**Figure 4a**). Meanwhile, the virtual electronic simulation of the two coin cell proton batteries connected in series with the LED showed that the green LED was brightly lit with an output voltage of 2.1 V (**Figure 4b**). At the end of the simulation, the output voltage decreased in accordance with the actual output voltage (**Figure 4c**). The initial output voltage of the simulation was slightly lower compared to the actual output voltage. After 10 hours, the voltages of both proton batteries continued to decrease to 100 hours (**Figure 4d**).

The output voltage of the actual functioning and simulation of the coin cell proton batteries should be similar with the nominal voltage of a commercial Zn-MnO_2 battery (1.5 V). Hence, the combination of two coin cell proton batteries in series with an LED should give a nominal voltage of 3.0 V. However, the initial voltage for the actual functioning was slightly lower, and this was attributed to several factors, such as the anode material, type of electrolyte and weight of the anode. Meanwhile, the initial output voltage of the simulation was lower due to the limitation of the MULTISIM software, similar to a previous study on simulation for PEMFC [41].

4. Conclusion

The PCA and PCA-5A membranes were successfully characterized by their functional groups, and thermal and tensile properties. All the characterization results confirmed that the PCA-5A membrane has good electrolyte properties. The correlation between the actual and simulation performance proved that the PCA-5A membrane is suitable for use as an electrolyte for proton batteries.

Acknowledgements

SSA would like to thank MyPhD scholarship, while AAM and ZMA extend their appreciation to ERGS (203/PBAHAN/6730006) for their financial support.

References

1. A. Khiar, R. Puteh, A. Arof, Physica B: Condensed Matter 373 (2006) 23-27.
2. L.S. Ng, A.A. Mohamad, J. Power Sources 163 (2006) 382-385.
3. S.R. Majid, A.K. Arof, Physica B: Condensed Matter 390 (2007) 209-215.
4. L.S. Ng, A.A. Mohamad, J. Membr. Sci. 325 (2008) 653-657.
5. M.H. Buraidah, L.P. Teo, S.R. Majid, A.K. Arof, Physica B: Condensed Matter 404 (2009) 1373-1379.
6. S.R. Majid, N.H. Idris, M.F. Hassan, T. Winie, A.S.A. Khiar, A.K. Arof, Ionics 11 (2005) 451-455.
7. J. Wang, Y. Zhang, H. Wu, L. Xiao, Z. Jiang, J. Power Sources 195 (2010) 2526-2533.
8. J.A. Seo, J.H. Koh, D.K. Roh, J.H. Kim, Solid State Ion. 180 (2009) 998-1002.
9. Y. Wan, K.A.M. Creber, B. Peppley, V.T. Bui, J. Membr. Sci. 284 (2006) 331-338.
10. M. Shukur, M. Kadir, Electrochim. Acta 158 (2015) 152-165.
11. Y. Yusof, H. Illias, M. Kadir, Ionics 20 (2014) 1235-1245.
12. D.E.S. Santos, C.G.T. Neto, J.L.C. Fonseca, M.R. Pereira, J. Membr. Sci. 325 (2008) 362-370.
13. S.S. Alias, Z.M. Ariff, A.A. Mohamad, Ceram. Int. 41 (2015) 5484-5491.
14. S.S. Alias, Z.M. Ariff, A.A. Mohamad, Int. J. Electroactive Mater 3 (2015) 33-37.
15. J. Ma, Y. Sahai, Carbohydr. Polym. 92 (2013) 955-975.
16. H. Bai, H. Zhang, Y. He, J. Liu, B. Zhang, J. Wang, J. Membr. Sci. 454 (2014) 220-232.
17. N.A. Aziz, S.R. Majid, A.K. Arof, J. Non-Cryst. Solids 358 (2012) 1581-1590.
18. N.N. Mobarak, A. Ahmad, M.P. Abdullah, N. Ramli, M.Y.A. Rahman, Electrochim. Acta 92 (2013) 161-167.
19. A. Pawlicka, R.I. Mattos, C.E. Tambelli, I.D.A. Silva, C.J. Magon, J.P. Donoso, J. Membr. Sci. 429 (2013) 190-196.
20. Y.N. Sudhakar, M. Selvakumar, Electrochim. Acta 78 (2012) 398-405.
21. S.S. Alias, S.M. Chee, A.A. Mohamad, Arab. J. Chem. 2014; In Press, Accepted Manuscript (http://dx.doi.org/10.1016/j.arabjc.2014.05.001) (2014).
22. A. Jamaludin, A.A. Mohamad, J. Appl. Polym. Sci. 118 (2010) 1240-1243.
23. M.F.Z. Kadir, S.R. Majid, A.K. Arof, Electrochim. Acta 55 (2010) 1475-1482.
24. M.F. Shukur, R. Ithnin, H.A. Illias, M.F.Z. Kadir, Opt. Mater. 35 (2013) 1834-1841.
25. H. Hu, J.H. Xin, H. Hu, A. Chan, L. He, Carbohydr. Polym. 91 (2013) 305-313.
26. T. Gümüşoğlu, G.A. Arı, H. Deligöz, J. Membr. Sci. 376 (2011) 25-34.
27. M.S. Bostan, E.C. Mutlu, H. Kazak, S. Sinan Keskin, E.T. Oner, M.S. Eroglu, Carbohydr. Polym. 102 (2014) 993-1000.
28. M.F.Z. Kadir, Z. Aspanut, S.R. Majid, A.K. Arof, Spectrochim. Acta, Part A 78 (2011) 1068-1074.
29. C. Tang, N. Chen, Q. Zhang, K. Wang, Q. Fu, X. Zhang, Polym. Degrad. Stab. 94 (2009) 124-131.
30. M.K. Trivedi, A. Branton, D. Trivedi, G. Nayak, K. Bairwa, S. Jana, Mod. Chem. Appl. 3 (2015) 1-6.
31. S. Hashmi, A. Kumar, K. Maurya, S. Chandra, J. Phys. D: Appl. Phys. 23 (1990) 1307-1314.
32. G. Inzelt, M. Pineri, J. Schultze, M. Vorotyntsev, Electrochim. Acta 45 (2000) 2403-2421.
33. A.-C. Dupuis, Prog. Mater Sci. 56 (2011) 289-327.
34. J. Wang, H. Zhang, Z. Jiang, X. Yang, L. Xiao, J. Power Sources 188 (2009) 64-74.
35. Z. Osman, A.K. Arof, Electrochim. Acta 48 (2003) 993-999.
36. J. Zhang, S. Chen, X. Xie, K. Kretschmer, X. Huang, B. Sun, G. Wang, J. Membr. Sci. 472 (2014) 133-140.
37. C.M. Costa, L. Rodrigues, V. Sencadas, M. Silva, J.G. Rocha, S. Lanceros-Méndez, J. Membr. Sci. 407 (2012) 193-201.
38. B. Zhang, Q. Wang, J. Zhang, G. Ding, G. Xu, Z. Liu, G. Cui, Nano Energy 10 (2014) 277-287.
39. N.A. Choudhury, J. Ma, Y. Sahai, J. Power Sources 210 (2012) 358-365.
40. M.F. Musameh, N. Anani, D. Smith, A programmable generic smart battery management system, in: 9th International Symposium on Communication Systems, Networks & Digital Sign (CSNDSP), IEEE, 2014, pp. 815-819.
41. M. Alberro, F.F. Marzo, A.P. Manso, V. Domínguez, J. Barranco, X. Garikano, Int. J. Hydrogen Energy 40 (2015) 3708-3718.